

Chapter 1 Methods for Laser Cooling of Solids

1.1 Introduction

The topic of laser cooling began with the articles of Pringsheim¹ and Hansch² long before any laboratory experiments were undertaken. These early papers proposed the use of optical radiation to remove energy from matter for the purpose of refrigeration, but the mere idea that light could transport thermal energy was widely doubted until Landau's thermodynamic analysis showed that radiation fields had entropy that depended on the statistics and mode structure of the field³. The influence of various states of the field on solid state cooling was examined in detail later⁴, but once it was realized that entropy of fields could be exchanged for entropy of matter the stage was already set for a concerted worldwide effort to alter the temperature of collections of atoms with light.

Experiments to observe laser cooling of atomic motion in gases originated from investigations of the mechanical effects of radiation pressure on small dielectric particles⁵. Similarly, optical refrigeration of solids was preceded by demonstrations that the amplitude of axial vibrations of mirrors could be reduced in Fabry-Perot resonators⁶. Reductions of this kind were accomplished by monitoring excursions of the cavity from resonance and using the error signal to control mirror position with variations of light pressure applied to the back side of one of the cavity mirrors. However this type of opto-mechanical feedback does not lead to overall refrigeration because it does not reduce the amplitude of internal modes of vibration irreversibly. Some modes are heated while others are cooled. To refrigerate a solid, light must do more than redistribute vibrational energy among the available modes. Ideally a low entropy (single-mode) input field couples to one or more vibrational or translational modes, undergoes an increase in entropy during its interaction with the sample, and then carries that entropy away via radiative transport into space.

Laser cooling techniques for solids can build on past experience in atomic vapors. In gases the motion of atoms along a chosen direction can be exploited to shift "hot" atoms preferentially into resonance with light propagating opposite to their motion via the Doppler effect⁷. In this way the momentum of the light wave is transferred to fast-moving atoms selectively, gradually slowing them down through the accumulated effect of many opposing photon interactions. In condensed matter however, free translational motion is absent. As a consequence, one might think that laser cooling in glasses or crystals has to exploit completely different principles. Yet there are analogies to the Doppler effect in solids and ways to address the energy and momentum of collective excitations of the medium that are reminiscent of interactions with free atoms. Hence this chapter reviews several methods with this perspective in mind, attempting to profit from the earlier history of laser cooling in gases and to provide points of comparison between different techniques.

Researchers face the challenge of developing the most effective means of controlling the temperature of macroscopic objects with light. Success on this front will make possible the thermal management of hot spots in micro-mechanical or integrated electronic devices, improved operation of high power lasers through radiation-balancing, and low temperature operation of active devices in vacuum where cooling improves sensitivity but is only possible through radiative transport.

1.2. Cooling with Anti-Stokes Fluorescence

The earliest demonstration of optical refrigeration of a solid relied on inducing anti-Stokes fluorescence by simply tuning the wavelength of incident light to the "red" or low energy side of an impurity resonance⁸. When vibronic coupling of the medium is weak, the detuning is into the spectral wing of an essentially pure electronic transition. When the vibronic coupling is strong, a

condition characterized by a large Huang-Rhys factor⁹, the light is detuned into the phonon sideband associated with the electronic transition. Then, consistent with quantum theory¹⁰, the absorption of photons on the low energy side of resonance is followed on average by photon emission at the center frequency of the transition. In this circumstance an overall loss of energy is imposed even on stationary atoms (Fig. 1). Hence this general approach has met with considerable success in demonstrations of cooling in rare earth solids¹¹, liquids¹², semiconductors¹³, and internal acoustic modes of optomechanical resonators¹⁴.

The efficiency of cooling that relies on inducing anti-Stokes fluorescence can easily be estimated. In the 2-level system of Fig. 1, an amount of energy given by $h\nu$ is added to the system for each absorbed photon. Energy $h\nu_{fl}$ is removed by each fluorescent photon. Hence if these two steps account for all system dynamics, then an input power of P_{in} produces a cooling power per absorbed photon of

$$P_c = P_{in} \left(\frac{\nu_{fl} - \nu_L}{\nu_L} \right), \quad (1)$$

and the cooling efficiency would be $\eta = P_c / P_{in} = (\nu_{fl} - \nu_L) / \nu_L$. However in the presence of non-radiative relaxation, which is commonplace in rare earth solids, the radiative quantum efficiency is lowered. Radiative and non-radiative decay at rates W_r and W_{nr} then contribute an external efficiency factor of the form $\eta_{ext} = W_r / (W_r + W_{nr})$. When corrected for fluorescence escape efficiency η_e , which is the fraction of emitted photons that escape the sample, this factor becomes

$$\eta_{ext} = \eta_e W_r / (\eta_e W_r + W_{nr}). \quad (2)$$

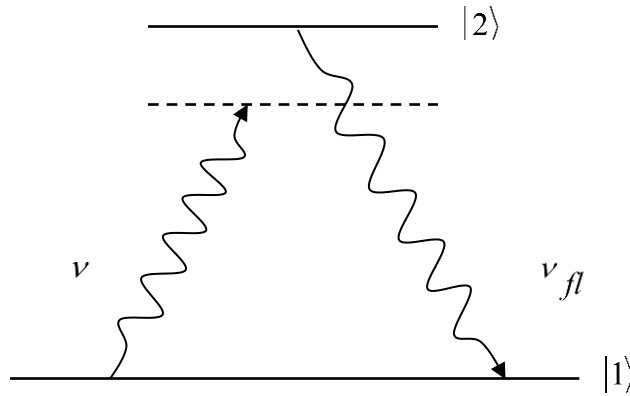


Figure 2. Anti-Stokes fluorescence emission in a 2-level system.

Additionally, only a fraction of the absorbed photons result in excitation of coolant atoms. The rest are absorbed by background impurities. With the absorption coefficient of the coolant atoms designated by α_c and that of the background by α_b , the proportion of absorbed photons that contribute to cooling is

$$\eta_{abs} = \frac{\alpha_c}{(\alpha_c + \alpha_b)}. \quad (3)$$

If the assumption is made that phonon-mediated absorption is proportional to the occupation probability of the phonon mode, namely $\langle n \rangle = (\exp[\hbar\Omega/k_B T] - 1)^{-1}$, the efficiency becomes $\eta_{abs} = \alpha_c \langle n \rangle / (\alpha_c \langle n \rangle + \alpha_b)$. Then at high temperatures ($k_B T \gg \hbar\Omega$), η_{abs} varies little with temperature when the background absorption is low ($\alpha_b / \alpha_c \ll 1$). On the other hand at low temperatures, as $\langle n \rangle \rightarrow 0$, η_{abs} decreases in proportion to $\langle n \rangle$. Hence the absorption efficiency drops dramatically through the important cryogenic regime. The overall cooling is determined by the product of the various efficiency factors.

$$\eta_c = \eta_{ext} \eta_{abs} \left(\frac{\nu_{fl} - \nu}{\nu} \right) \quad (4)$$

From (1) and (4) it is easy to show that the cooling power density per unit frequency is $P_c/V = \eta_{abs} \eta_{ext} \alpha_{tot} I_\nu (\nu_{fl} - \nu) / \nu$. Here $I_\nu = I_0 g(\nu)$ is the intensity per unit frequency and $g(\nu)$ is a normalized spectral lineshape function. V is the interaction volume. If the bandwidth of the light source equals the full linewidth 2Γ of the optical transition, and the density of atoms in the interaction volume is N/V , the energy loss rate per atom is

$$R = 2\Gamma \eta_c \alpha_{tot} I_\nu (V/N) = \eta_c \alpha_{tot} I_0 (V/N). \quad (5)$$

The condition for net cooling can be expressed in a simple way based on Eq. (4), since η_c must exceed zero. By assuming that the laser detuning is optimized at the phonon frequency Ω , we can rewrite the numerator using $h\nu_{fl} - h\nu = \hbar\Omega$. Furthermore the average phonon energy is $\hbar\Omega \cong k_B T$ near the boundary of the classical regime¹⁵. Then the condition for laser cooling ($\eta_c > 0$) becomes

$$\eta_{ext} \eta_{abs} > 1 - \frac{k_B T}{h\nu}. \quad (6)$$

An important limitation of refrigeration based on anti-Stokes fluorescence emerges from this condition by determining the temperature at which the cooling efficiency drops to zero ($\eta_c = 0$). By solving (6) as an equality, it is found that a lower bound exists for the attainable temperature. The minimum temperature T_{min} that can be reached with anti-Stokes cooling found from (6) is

$$T_{min} = \frac{h\nu}{k_B} \left(\frac{(\alpha_b / \alpha_c) + (1 - \eta_{ext})}{1 + (\alpha_b / \alpha_c)} \right). \quad (7)$$

According to (7), if the quantum efficiency is high ($\eta_{ext} \cong 1$), the temperature limit for laser cooling by anti-Stokes emission is primarily determined by the frequency of light and the ratio of background to resonant absorption. The dependence on these two factors arises because heat input to the system is proportional to incident photon energy and absorptive heating efficiency. Only when the background absorption coefficient vanishes could arbitrarily low temperatures be reached. For the moderate levels of background absorption encountered in practice in solids, this places a severe constraint on temperatures that can be reached by laser cooling. As a simple example of this, the anti-Stokes cooling limit predicted by (7) at a wavelength of 1 micron is $T_{min} = 145.3\text{K}$ when the external quantum efficiency is $\eta_{ext} = 0.90$ and background absorption coefficient is $\alpha_b = \alpha_c / 1000$.

The lower bound on attainable temperatures can be interpreted in another way. It arises because the cooling rate depends on phonon occupation, a factor which diminishes as temperature decreases. Eventually the rate of anti-Stokes cooling drops below the rate of heating from background impurity absorption and cooling is no longer possible¹⁶. For 3-D refrigeration of solids to be as effective as laser cooling of gases, techniques capable of maintaining high rates of cooling through the cryogenic temperature range are needed. This is discussed further in what follows.

In the remainder of this chapter momentum is incorporated into the discussion to investigate whether the fundamental temperature limitation of anti-Stokes fluorescence cooling can be evaded when the dynamics are viewed comprehensively. Judging from the successes of laser cooling of gases, cooling schemes that conserve momentum and energy simultaneously during optical interactions are the most efficient. Yet momentum is disregarded in the anti-Stokes fluorescence method. Other techniques may offer the capability of balancing the momentum and energy requirements more consistently to accommodate phonon dispersion (Fig. 2).

1.3 Brillouin Cooling

In gases the link between linear momentum and the absorption of a photon is simple. For each photon absorbed, the linear momentum of an approaching atom decreases by an average of $\hbar k$. Translational momentum is thereby reduced, provided fluorescence randomizes the direction of re-emitted photons. In solids things are not so simple because free translation of atoms cannot take place. Atomic displacements are oscillatory. Motion is conveyed in collective waves and momentum is distributed as illustrated in Fig. 2. Nevertheless, charge motions associated with departures of atoms from their equilibrium positions have Fourier components with well-defined amplitude, momentum, and energy¹¹. Moreover, Doppler-shifted interactions with these phonon

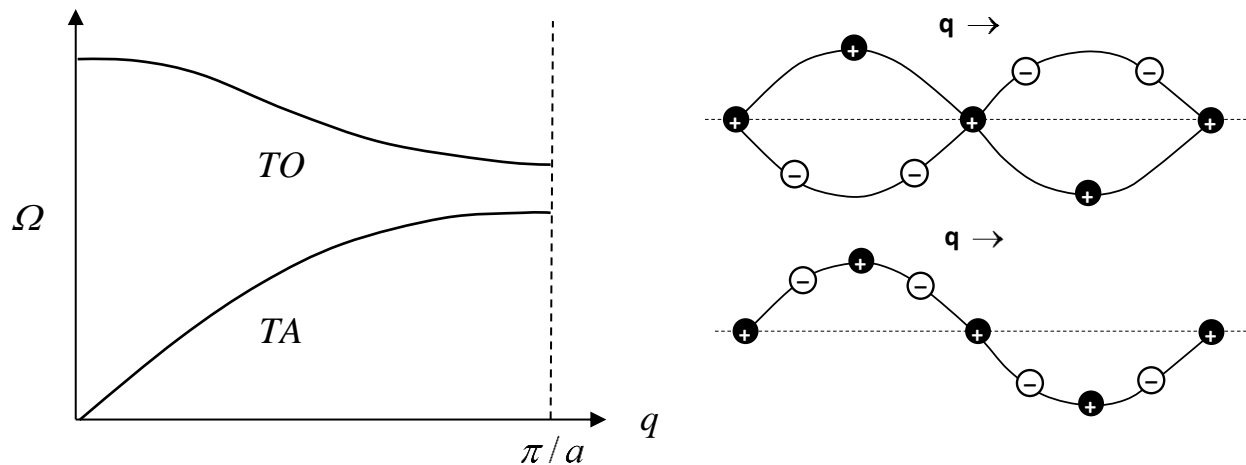


Figure 2. (Left) Dispersion curves illustrating the variation of phonon frequency Ω with wavevector q for transverse acoustic (TA) and optic modes (TO). The lattice constant is a . (Right) Particle displacements in a diatomic linear lattice for TO (upper) and TA (lower) modes of the same wavelength.

modes are well-known to take place in acousto-optic (Brillouin) scattering¹⁵. So analogies to Doppler cooling methods in gases are useful. At this point we therefore formulate the problem of light interacting with acoustic and optical modes of vibration in terms of interaction Hamiltonians and equations of motion that display momentum explicitly. Two recent developments are reviewed.

The most detailed consideration is given to laser cooling by stimulated Raman scattering because in theory it furnishes a cooling rate that is independent of temperature.

The energy of interaction between light and a solid derives from the electron-phonon interaction in which the force of light acts to displace ions from equilibrium by an amount $\delta\bar{R}(t)$. This displacement can be written as a Fourier expansion in terms of normal modes of polarization $\hat{\varepsilon}_{k\lambda}$ ($\lambda = 1,2,3$), amplitude $Q_{q\lambda}$, wavevector \bar{q} and frequency $\Omega_{q\lambda}$. For an ion situated at equilibrium position \bar{R}_0 in a solid, undergoing motion described by a single phonon mode, the displacement consists of only one Fourier term.

$$\delta\bar{R}(t) = (NM)^{-1/2} Q(\Omega, t) \hat{\varepsilon} \exp[i\bar{q} \cdot \bar{R}_0]. \quad (8)$$

$\hat{\varepsilon}$ is the polarization vector, N is the number of particles, and M is the particle mass. The form of the interaction Hamiltonian is given by force times distance.

$$H_I = -\bar{\nabla}V \cdot \delta\bar{R} \quad (9)$$

The quantized form of H_I depends on the coupling mechanism between light and the vibrational mode of interest, so the cases of acoustic and optical vibrational modes are considered separately below.

For transverse *acoustic modes*, which are propagating density fluctuations, the light-matter interaction is determined by electrostrictive deformations of the medium because transverse optical fields cannot couple directly to longitudinal waves. The energy dependence of acoustic and optical modes on wavevector is shown in Fig. 2. To generate pressure waves, a deformation potential¹⁷ is needed of the form

$$\bar{\nabla}V = -\gamma\bar{\nabla}(\bar{E}_1 \cdot \bar{E}_2^*) = -\gamma q E_1 E_2^* \hat{\varepsilon}. \quad (10)$$

Here

$$E_1(z, t) = \xi_k (\hat{a}_1^- e^{-i(\omega_1 t - kz)} + \hat{a}_1^+ e^{i(\omega_1 t - kz)}) \quad (11)$$

and

$$E_2^*(z, t) = \xi_{k+q} (\hat{a}_2^+ e^{i(\omega_2 t - [k+q]z)} + \hat{a}_2^- e^{-i(\omega_2 t - [k+q]z)}) \quad (12)$$

are quantized pump and anti-Stokes fields, $\xi_k = \sqrt{\hbar\omega_k / 2\varepsilon_0 V}$ is the field per photon, and $\gamma \equiv [\rho(\partial\varepsilon / \partial\rho)]_{\rho_0}$ is the electrostrictive constant relating changes of permittivity to changes of density¹⁸. The operator for normalized mode amplitude is related to the phonon creation (\hat{b}^+) and annihilation (\hat{b}^-) operators by

$$\hat{Q}(\Omega, t) = \left(\frac{\hbar}{2\Omega}\right)^{1/2} (\hat{b}_q^- \exp[-i\Omega t] + \hat{b}_q^+ \exp[i\Omega t]). \quad (13)$$

When Eqs. (8, 10-13) are combined with (9) the interaction Hamiltonian becomes

$$\begin{aligned} H_I &= -(NM)^{-1/2} (\hat{\varepsilon} \cdot \bar{\nabla}V) Q(\Omega, t) \exp[i\bar{q} \cdot \bar{R}_0] \\ &= \hbar f (\hat{b}_q^- \hat{a}_{k+q}^+ \hat{a}_k^- + h.c.), \end{aligned} \quad (14)$$

where the interaction strength is defined as $f \equiv (2\hbar NM\Omega)^{-1/2} V\gamma q \xi_k \xi_{k+q}$. V is the volume of interaction. The conservation of momentum in the interaction is illustrated in Fig. 3.

The Hamiltonian can be used to calculate temporal changes in the vibrational energy (or temperature) of the medium. To appreciate the connection between H_I and vibrational energy or temperature, note that the conjugate momentum of the vibrational amplitude $\hat{Q}(\Omega, t)$ is

$$\hat{P}(\Omega, t) = -i \left(\frac{\hbar \Omega}{2} \right)^{1/2} (\hat{b} \exp[-i\Omega t] - \hat{b}^+ \exp[i\Omega t]). \quad (15)$$

When \hat{Q} and \hat{P} are defined as above, the single mode Hamiltonian specifying vibrational energy reduces to a familiar form.

$$H_{q\lambda} = \frac{1}{2} (\hat{P}_{q\lambda}^+ \hat{P}_{q\lambda} + \Omega_{q\lambda}^2 \hat{Q}_{q\lambda}^+ \hat{Q}_{q\lambda}) = \frac{1}{2} \hbar \Omega_{q\lambda} (\hat{b}_{q\lambda}^+ \hat{b}_{q\lambda}^- + h.c.). \quad (16)$$

Taking all possible modes into account, the total energy is therefore found to be

$$H = \sum_{q,\lambda} H_{q\lambda} = \sum_{q,\lambda} \hbar \Omega_{q\lambda} (\hat{b}_{q\lambda}^+ \hat{b}_{q\lambda}^- + \frac{1}{2}). \quad (17)$$

Since $\langle \hat{n}_{q\lambda} \rangle = \langle \hat{b}_{q\lambda}^+ \hat{b}_{q\lambda}^- \rangle$ is the number of phonons in mode q , the summation in Eq. (17) describes the total vibrational energy of the medium as a weighted sum of the individual mode energies which in turn determines the sample temperature.

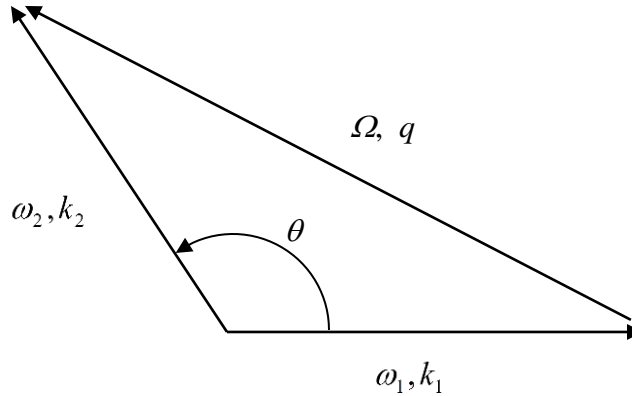


Figure 3. Wavevector diagram for phonon scattering through angle θ . Phonon frequency Ω and wavevector $\bar{q} = \bar{k}_2 - \bar{k}_1$ conserve energy and linear momentum in the wave interaction involving optical fields $\bar{E}_1(\omega_1)$ and $\bar{E}_2(\omega_2)$.

With the interaction Hamiltonian of Eq. (14) in hand, optically-driven dynamics of two optical waves interacting with an acoustic mode can be analyzed. The static Hamiltonian $H_0 = \hbar \omega_1 \hat{a}_1^+ \hat{a}_1^- + \hbar \omega_2 \hat{a}_2^+ \hat{a}_2^- + \hbar \Omega \hat{b}^+ \hat{b}^-$ plays no role in steady-state dynamics. For example the change of phonon occupation with time can be calculated using the Heisenberg equation of motion

$$\begin{aligned} \dot{\hat{n}}_b &= (i/\hbar)[H_0 + H_{\text{int}}, \hat{n}] \\ &= (i/\hbar) \left\{ \hbar f (\hat{b}^- \hat{a}_2^+ \hat{a}_1^- + h.c.), \hat{b}^+ \hat{b}^- \right\} \\ &= if \left\{ \hat{b}^- \hat{a}_2^+ \hat{a}_1^- (\hat{b}^+ \hat{b}^-) - \hat{b}^+ (\hat{b}^- \hat{b}^+) \hat{a}_2^- \hat{a}_1^+ \right\}. \end{aligned} \quad (18)$$

The first term on the right determines the rate of annihilation of phonons while the second term is the rate of creation. We can show this explicitly by solving for the temporal behavior of \hat{b}^+ and \hat{b}^- , again using the Heisenberg picture.

$$(d\hat{b}^+ / dt) = i\Omega \hat{b}^+ + if \hat{b}^- \hat{a}_1^- \hat{a}_2^+ \hat{b}^+ - if \hat{b}^+ \hat{a}_1^+ \hat{a}_2^- \hat{b}^- - \Gamma_b \hat{b}^+ \quad (19)$$

$$(d\hat{b}^- / dt) = -i\Omega \hat{b}^- - if \hat{b}^+ \hat{a}_1^+ \hat{a}_2^- \hat{b}^- + if \hat{b}^- \hat{a}_1^- \hat{a}_2^+ \hat{b}^+ - \Gamma_b \hat{b}^- \quad (20)$$

Making use of the Slowly-Varying Envelope Approximation (S.V.E.A.), steady-state solutions for the operator amplitudes are simply

$$\hat{b}^+ = \{if\hat{b}^-\hat{a}_1^-\hat{a}_2^+\hat{b}^+ - if\hat{b}^+\hat{a}_1^+\hat{a}_2^-\hat{b}^-\}/\Gamma_b, \quad (21)$$

$$\hat{b}^- = \{-if\hat{b}^+\hat{a}_1^+\hat{a}_2^-\hat{b}^- + if\hat{b}^-\hat{a}_1^-\hat{a}_2^+\hat{b}^+\}/\Gamma_b. \quad (22)$$

With these substitutions one finds that the net rate of change of phonon occupation in the state $|n_1\rangle|n_2\rangle|n_b\rangle$ is determined by the balance of annihilation versus creation.

$$\begin{aligned} \langle \dot{n}_b \rangle = & if \langle n_b | \langle n_1 | \langle n_2 | \{-if\hat{b}^+\hat{a}_1^+\hat{a}_2^-\hat{b}^- + if\hat{b}^-\hat{a}_1^-\hat{a}_2^+\hat{b}^+\} \hat{a}_2^+\hat{a}_1^-(\hat{b}^+\hat{b}^-) | n_2 \rangle | n_1 \rangle | n_b \rangle / \Gamma_b \\ & - if \langle n_b | \langle n_1 | \langle n_2 | \{if\hat{b}^-\hat{a}_1^-\hat{a}_2^+\hat{b}^+ - if\hat{b}^+\hat{a}_1^+\hat{a}_2^-\hat{b}^-\} \hat{a}_2^-\hat{a}_1^+(\hat{b}^-\hat{b}^+) | n_2 \rangle | n_1 \rangle | n_b \rangle / \Gamma_b \end{aligned} \quad (23)$$

Upon evaluation of the matrix elements we obtain the rate equation for phonon occupation.

$$\dot{n}_b = -(f^2/\Gamma_b)n_1(n_2+1)n_b + (f^2/\Gamma_b)(n_1+1)n_2(n_b+1). \quad (24)$$

The first term on the right side of Eq. (24) describes cooling while the second describes heating. Possible detuning of the modes has been ignored in this analysis. The phonon annihilation rate for resonant Brillouin scattering in the interaction volume is therefore the coefficient of the first term in (24).

$$\gamma_B = (f^2/\Gamma_b)n_1(n_2+1)n_b \quad (25)$$

The energy loss rate takes into account the phonon frequency.

$$R = \gamma_B \hbar \Omega = (f^2/\Gamma_b)n_1(n_2+1)n_b \hbar \Omega. \quad (26)$$

Laser cooling is realized if conversion of an optical pump wave to an anti-Stokes wave prevails over its conversion to a Stokes-shifted wave¹⁹. Brillouin cooling of a mechanical mode was first demonstrated in a micro-resonator by simultaneously matching its momentum and energy to the difference of wavevectors and frequencies of the pump and anti-Stokes waves¹⁴. To do this the pump and anti-Stokes waves were simultaneously enhanced in the resonator while the Stokes component of Brillouin scattering was suppressed by wavevector mismatch.

1.4 Raman Cooling

In this section stimulated scattering is considered for the cooling of solids. The general theory of stimulated Brillouin and Raman scattering^{20,21} was developed in the 1960s and despite the complexity of equations coupling the various mode amplitudes Louisell²² pointed out that the interaction energy is just the added electromagnetic energy resulting from a change in the permittivity ε , or $H_I = \frac{1}{2} \int \delta\varepsilon E^2$. This perspective facilitates the analysis of both Brillouin and Raman scattering since it is straightforward to write $\delta\varepsilon$ to reflect one interaction or the other. In the last section the dielectric fluctuation in Brillouin scattering was written $\delta\varepsilon = -\gamma(\partial Q/\partial x)$ to describe electrostriction by the incident light. In this section $\delta\varepsilon$ arises from dielectric fluctuations due to transverse charge motion caused directly by the light field itself. We shall proceed as before nevertheless, writing down the interaction Hamiltonian using Eq. (9), since the deformation potential approach is equivalent to that of Louisell.

For transverse *optical modes*, the net optical electric field can act directly on charged ions at the difference frequency to create or destroy optical phonons. In this case the potential is just the optical energy density at the mode frequency. Hence the gradient of the potential in Eq. (9) is $\bar{\nabla}V = \varepsilon_0 \bar{\nabla}(\bar{E}_1 \cdot \bar{E}_2^*)\hat{\varepsilon}$, and the single mode interaction Hamiltonian is

$$\begin{aligned}
 H_I &= \left(\frac{\hbar \varepsilon_0^2}{2\Omega NM} \right)^{1/2} \xi_k \xi_{k+q} (\hat{a}_1^- \hat{a}_2^+ \hat{b}^- + h.c.) \\
 &= \hbar f' (\hat{a}_1^- \hat{a}_2^+ \hat{b}^- + h.c.)
 \end{aligned} \tag{26}$$

where $f' \equiv -(2\hbar NM\Omega)^{-1/2} \varepsilon_0 V q \xi_k \xi_{k+q}$ is the coupling strength in the interaction volume V . By careful selection of the frequencies and wavevectors of two optical fields, the energy and momentum can be conserved for optical modes just as for acoustic modes (Fig. 3).

Two-photon Raman transitions (Fig. 4) can couple to optical modes of vibration purely through anti-Stokes scattering. Consequently they can be utilized for efficient cooling. Early analysis and experiments on Raman cooling may be found in Refs. 23-25. Here we follow Ref. 26 to analyze how the Raman technique can be adapted to cooling solids and to estimate the cooling rate. The potential advantages of applying adiabatic rapid passage to this technique are also considered. The fact that the cooling rate is temperature independent is emphasized.

With pulsed excitation, the two fields at ω_1 and ω_2 in Fig. 4 cause the system population to evolve in the direction indicated by wiggly arrows. The light drives population from state 1 to state 3 at a rate determined by the one- and two-photon detunings Δ and δ . The $1 \rightarrow 2$ and $2 \rightarrow 3$ transitions are assumed to be electric-dipole allowed. The selection rules therefore dictate that state 3 is a long-lived storage state. For prolonged excitation, population builds up in level 3 and the reverse process begins to take place at a comparable rate. For the 2-photon detuning shown in the figure, a small energy deficit ($\hbar\delta$) and momentum reduction ($2\hbar k$) is incurred for each Raman cycle, provided the pulses are short enough to avoid substantial buildup of population²⁷ in state 3. Atoms with a velocity centered at $v = 2\hbar k/m$ lose kinetic energy. By emptying state 3 periodically with a fast, random process like fluorescence, changes in the energy and momentum distributions become irreversible through an increase in the entropy^{3,4} of the outgoing radiation field²⁸. Hence the ensemble of atoms can be progressively cooled.

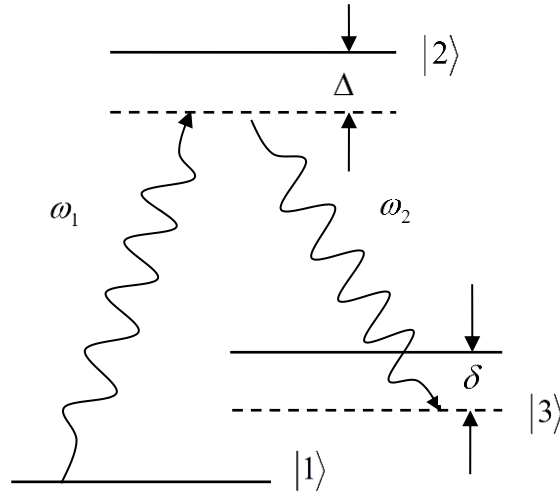


Figure 4. A 3-level system undergoing a 2-photon Raman process. $\Delta = \omega_{12} - \omega$ is the 1-photon detuning and $\delta = \omega_{13} - (\omega_1 - \omega_2)$ is the 2-photon detuning.

To estimate the stimulated Raman transition rate for the $1 \rightarrow 3$ transition it is instructive to develop a sense of the importance of "forward" and "backward" pumping processes between states 1

and 3 (Figures 4 and 5 respectively). It is easily shown that the net rate of change of population is zero in steady-state because of the balance of these two processes, which provide cooling and heating respectively. One can also show that the transition rate for a single process is given by the square of an off-diagonal (coherence) element of the density matrix that may be evaluated straightforwardly to allow estimation of cooling rates.

The net rate of population change in excited state 3 is just $\dot{\rho}_{33} \equiv d\rho_{33}/dt$. In the weak field limit the wavefunction is dominated by its ground state component, which varies little with time. Hence we may assume $\rho_{11} = c_1 c_1^* \cong 1$ in order to calculate the transition rate

$$\dot{\rho}_{33} = \frac{d}{dt} [\langle 3|\psi\rangle\langle\psi|3\rangle] \cong \frac{d}{dt} [\langle 3|c_3|3\rangle\langle 1|c_1^*c_1|1\rangle\langle 3|c_3^*|3\rangle] = \dot{\rho}_{31}\rho_{13} + \rho_{31}\dot{\rho}_{13}. \quad (27)$$

Since $\rho_{31} = \rho_{13}^*$ and $|\rho_{31}| = |\rho_{13}|$, one finds $\dot{\rho}_{31} = \dot{\rho}_{13}^* = -i\omega_{13}\rho_{31}$ and $\dot{\rho}_{13} = i\omega_{13}\rho_{13}$. The result is that the two contributions to ρ_{33} given in Eq. (27) are equal and opposite. Under steady-state conditions the occupation of state 3 therefore does not change.

$$\dot{\rho}_{33} = -i\omega_{13}|\rho_{13}|^2 + i\omega_{13}|\rho_{13}|^2 = 0 \quad (28)$$

The rate at which level 3 population increases is determined by the positive term in (28) assuming one vibrational quantum occupies the mode. The transition rate per atom per unit (angular frequency) excitation bandwidth that leads to cooling is therefore

$$|\dot{\rho}_{33}/\omega_{13}| = |\rho_{13}|^2. \quad (29)$$

To determine the rate itself from the field-driven coherence in (29) the source bandwidth must be specified. Taking this to equal the full transition linewidth $2\Gamma_{13}$ in the discussion below, it remains only to calculate the matrix element ρ_{13} explicitly.

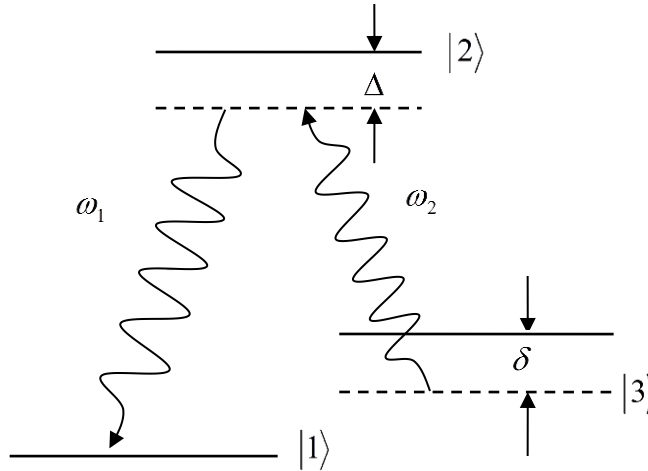


Figure 5. Raman interaction of fields $E_1(\omega_1)$ and $E_2(\omega_2)$ in time-reversed (“backward”) sequence.

For quasi, steady-state fields the interaction Hamiltonian can be written

$$V = (-\frac{1}{2}\hbar\Omega_{12}\exp(i\omega_1t) + c.c.) + (-\frac{1}{2}\hbar\Omega_{23}\exp(i\omega_2t) + c.c.). \quad (30)$$

Contributions to state 3 dynamics other than the one depicted in Fig. 4 will be ignored owing to their large detunings from resonance. The first order coherence is therefore given by the standard first order perturbation expression²⁹:

$$\tilde{\rho}_{12}^{(1)} = \left(\frac{\Omega_{12}/2}{\Delta_1 + i\Gamma_{12}} \right) (\rho_{11}^{(0)} - \rho_{22}^{(0)}). \quad (31)$$

The second order coherence established by the forward Raman process is obtained by solving the second order transport equation

$$i\hbar\dot{\rho}_{13}^{(2)} = \hbar(\omega_1 - \omega_3)\rho_{13}^{(2)} + [V^{(1)}, \rho^{(1)}]_{13} - i\hbar\Gamma_{13}\rho_{13}^{(2)}. \quad (32)$$

The 2-photon coherence oscillates at the frequency of the (combined) driving fields. So if the slowly-varying envelope approximation is adopted, the form of ρ_{13} is

$$\rho_{13}^{(2)}(t) = \tilde{\rho}_{13}^{(2)} \exp[i(\omega_1 - \omega_2)t]. \quad (33)$$

By substituting Eqs. (30), (31) and (33) into (32) and grouping terms with the same time dependence, one finds the solution for the coherence to be

$$\tilde{\rho}_{13}^{(2)} = \left\{ \left(\frac{\Omega_{12}\Omega_{23}^*/4}{[\Delta_1 + i\Gamma_{12}][\Delta_2 + i\Gamma_{13}]} \right) (\rho_{11}^{(0)} - \rho_{22}^{(0)}) \right\}. \quad (34)$$

The second denominator incorporates the 2-photon detuning $\Delta_2 \equiv \omega_{31} - (\omega_1 - \omega_2)$. Using this result in Eq. (29), the Raman transition rate per atom is obtained with an appropriate assumption regarding excitation bandwidth. If the excitation matches the bandwidth of the Raman transition ($2\Gamma_{13}$), the number of phonon annihilations per impurity atom per second is

$$\gamma_R = 2\Gamma_{13} \langle n \rangle |\tilde{\rho}_{13}^{(2)}|^2 = 2\Gamma_{13} \langle n \rangle |\langle f|M|i \rangle|^2, \quad (35)$$

where adjustment has been made for the number of phonons occupying the mode using the Planck distribution $\langle n \rangle = (\exp[\hbar\Omega/k_B T] - 1)^{-1}$. In this model the implicit summation over intermediate states in the matrix element $\langle f|M|i \rangle$ reduces to a single term:

$$\langle f|M|i \rangle = \left[\frac{\langle 3|\mu^{(e)} \cdot \hat{e}_2|2\rangle \langle 2|\mu^{(e)} \cdot \hat{e}_1|1\rangle}{[\Delta_1 + i\Gamma_{12}][\Delta_2 + i\Gamma_{13}]} \right] \frac{E(\omega_1)E^*(-\omega_2)}{4\hbar^2}. \quad (36)$$

The rate of energy loss is therefore

$$R = \gamma_R \hbar\Omega = 2\Gamma_{13} \langle n \rangle |\langle f|M|i \rangle|^2 \hbar\Omega. \quad (37)$$

This rate applies to each atom in the interaction volume because it was calculated using the density matrix which is normalized to the number of coolant ions. To realize this cooling rate in practice, the optical interaction must be made irreversible. To this point, the dynamics we have described are coherent and proceed as readily in the “forward” direction as the “backward” direction. We must ensure that the second term in (27) describing reverse transitions is negligible. Also the overall efficiency may benefit from interaction with more than one mode at a time. So we briefly consider these aspects of Raman cooling next with the aid of Fig. 6.

Refrigeration requires irreversibility. The coherent (reversible) Raman process outlined above must therefore be combined with a random process that increases the entropy of outgoing radiation⁴ without decreasing efficiency. For this purpose fluorescence on an allowed transition at frequency ω_4 can be induced by a strong “repump” beam (at frequency ω_3) as illustrated schematically in Fig. 6. To avoid lowering the rate of cooling set by anti-Stokes Raman transitions, the return of excited state population to the ground state should be fast. Provided state 3 is emptied at a rate faster than the Raman excitation process which fills it, and no extra heat is generated in the process, efficient cooling will be maintained.

Improvement in the Raman cooling rate can be anticipated by interacting with a range of vibrational modes during each cooling cycle. More than one mode could be addressed for example by rapid scanning the 2-photon detuning δ in discrete steps²⁷ or by using some form of adiabatic passage. Reversal of the temporal order of two fixed frequency pulses can transfer population between two discrete states with nearly unit efficiency at a fixed detuning. However for rapid cooling over a broad range of phonon frequencies, rapid adiabatic passage is a superior method in which the excitation detuning is swept from one side of Raman resonance to the other adiabatically. This approach can be implemented very simply by imposing a "chirp" on $\delta(t)$. By sweeping the frequency rapidly from one side of resonance to the other, all phonons with frequencies between the endpoints $\pm \delta_{\max}$ of the chirp are cooled at once³⁰.

The need to avoid heat generation during the repump cycle affects how closely the repump beam may be tuned to resonance. The criterion for optimizing one-photon detuning in Raman cooling of solids is different from that for gases because the configuration of neighboring atoms surrounding a coolant atom changes as the dipole forms during transition of a coolant atom from a low to a high energy state. That is, the equilibrium positions of neighbors change in

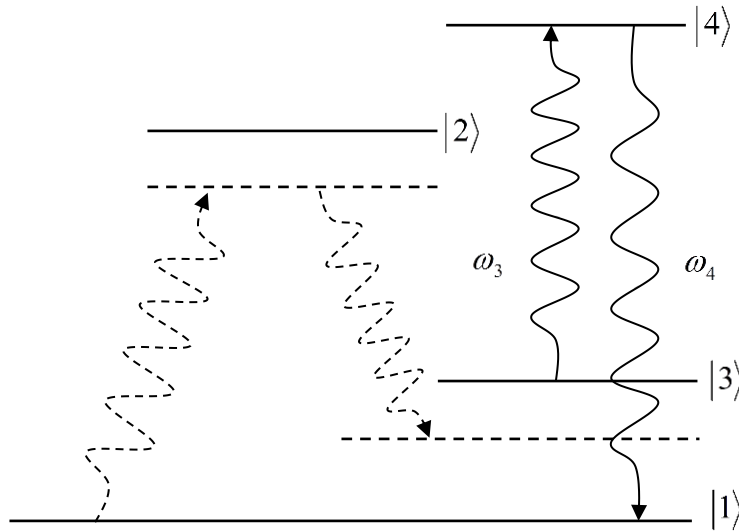


Figure 6. The coherent Raman process (dashed arrows) must be followed by random emission for there to be net cooling. Here, spontaneous emission is induced at ω_4 with a pump source at frequency ω_3 that returns population from state 3 to state 1.

response to the absorption process. Phonons are unavoidably generated by relaxation of this non-equilibrium configuration unless the light is detuned on the red side of resonance by more than the phonon energy.

In the illustration of Fig. 7, detuning requirements are considered in the context of energy levels of Ce^{3+} ions. Given the electronic structure of Ce^{3+} , the laser must be detuned by an amount equal to or greater than the Stokes shift of the longest wavelength $4f^{n-1} 5d \leftrightarrow 4f^n$ transition. For Ce^{3+} this means

$$\Delta_{\text{Laser}} \geq \Delta_{\text{Stokes}} + \Delta_F, \quad (38)$$

where Δ_F is the energy separating the ${}^2F_{5/2}$ and ${}^2F_{7/2}$ energy levels. This choice ensures that absorbed photons have less than the energy required to generate either a vibrationally-excited upper state or a vibrationally-excited ground state. In the Ce^{3+} system, cooling ought to maximize when both the Raman and repump beams are detuned by $\Delta_{\text{Laser}} = \Delta_{\text{Stokes}} + \Delta_F$. In practice, smaller detunings might improve the cooling if the transition rate from the 5d state to ${}^2F_{7/2}$ is less than that to ${}^2F_{5/2}$ as it is in Ce:YAG^{31} . Despite the reduction in cooling rate that large detunings incur in general, high overall cooling rates can be achieved when the excited state is exceptionally broad, as predicted²⁶ for the 5d state of Ce^{3+} .

To conclude this chapter we emphasize two key advantages of Raman cooling of solids, namely that the cooling rate is temperature independent and that the cooling process is divided into two main steps involving different levels, thereby permitting separate optimization of absorption and fluorescence. At low temperatures, the phonon occupation factor in Eq. (27) drops below one and varies as $\langle n \rangle \cong \exp(-\hbar\Omega/k_B T)$. In this non-classical regime, any cooling

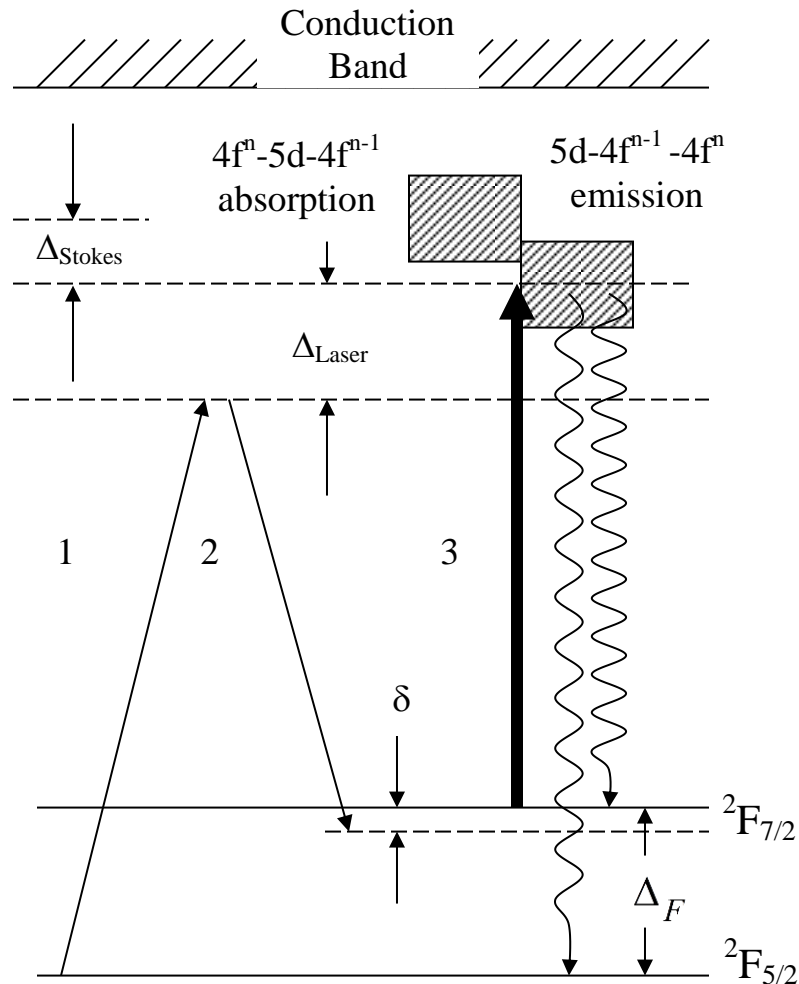


Figure 7. Energy levels and detunings involved in Raman laser cooling of a 3-level coolant atom in a solid. The example is based on the electronic structure of Ce^{3+} .

rate that is solely proportional to $\langle n \rangle$ falls exponentially as temperature decreases. Indeed γ_R is proportional to $\langle n \rangle$ according to Eq. (35), just like the rate for anti-Stokes fluorescence cooling. However the phonon-broadened linewidth Γ_{13} of the Raman transition is strongly temperature-dependent and offsets the decline with a matching proportionality to $\langle n \rangle$ of its own. In the model below there is complete cancellation of factors of $\langle n \rangle$ in Eq. (35) at 2-photon resonance. Since the transition to state 3 is detuned by the phonon frequency below the terminal electronic state (see Fig. 4), the relevant resonant condition is $\Delta_2 = 0$.

While other mechanisms may contribute, we assume here that the Raman linewidth is governed primarily by a 2-phonon Orbach process³². Thus it can be modeled as $\Gamma_{13}(T) \cong \Gamma_0(1 + \langle n \rangle[\Gamma'_0/\Gamma_0])$. In this expression Γ_0 is the limiting inhomogeneous linewidth at zero temperature. When $\Gamma'_0 > \Gamma_0$ the linewidth reduces to $\Gamma_{13}(T) \cong \langle n \rangle \Gamma'_0$. Upon substitution into Eq.(35) with zero 2-photon detuning ($\Delta_2 = 0$), the rate of phonon annihilation per atom becomes constant.

$$\gamma_R = \frac{2}{\Gamma'_0} |\langle f | M' | i \rangle|^2. \quad (39)$$

In this expression the modified matrix element M' appears because of the cancellation between $\langle n \rangle$ and 2-photon linewidth factors in the Orbach model outlined above. Its definition is

$$\langle f | M' | i \rangle = \left[\frac{\langle 3 | \mu^{(e)} \cdot \hat{e}_2 | 2 \rangle \langle 2 | \mu^{(e)} \cdot \hat{e}_1 | 1 \rangle}{[\Delta_1 + i\Gamma_{12}]} \right] \frac{E(\omega_1)E^*(-\omega_2)}{4\hbar^2}. \quad (40)$$

The energy loss rate per atom,

$$R = \gamma_R \hbar\Omega = \frac{2}{\Gamma'_0} |\langle f | M' | i \rangle|^2 \hbar\Omega, \quad (41)$$

is similarly expected to be temperature independent over the entire range $k_B T > \hbar\Gamma_0$. Unlike acoustic modes, optical phonons have very little dispersion (Fig. 2). Consequently the frequency of the dominant optical phonon does not vary significantly and R remains constant over a wide range of temperature.

The one-dimensional Raman interaction described above involves a phonon near the center of the Brillouin zone propagating along a single optical axis. However zone center phonons cannot participate directly in the collisional processes that establish thermal equilibrium within the phonon distribution. Hence it is natural to inquire as to how effectively a mode that is cooled irreversibly can equilibrate with the reservoir of other phonons in the solid. Restoration of equilibrium in solids is governed by Umklapp processes, phonon collisions requiring a reciprocal lattice vector \bar{G} to conserve momentum³³. Zone center phonons have low wavevectors, so when two phonons interact with a third via an Umklapp process, there is no way to satisfy the relation $\bar{k}_1 + \bar{k}_2 = \bar{k}_3 + \bar{G}$ with a wavevector \bar{G} that spans the entire Brillouin zone. To achieve uniform cooling of even a single mode, phonons propagating along orthogonal axes should be addressed, and this calls for the introduction of two more sets of counter-propagating Raman beam pairs to cover all three orthogonal space axes. Additionally, beam switching along each axis is needed to interrogate both forward- and backward-travelling phonons of the same frequency. Fast directional switching of each beam pair can be implemented with a Pockel's cell

that reverses the propagation direction of the ω_1 and ω_2 beams simultaneously within the sample²⁸ on a timescale much shorter than the lifetime of the $^2F_{7/2}$ shelving state.

While uniform cooling of one mode can be assured by such procedures, thermal equilibration of the sample as a whole relies on Umklapp processes that involve phonons of wavevector \bar{G} . Although the occupation probability of such phonons drops exponentially with decreasing temperature, the thermal conductivity which is proportional to phonon mean free path actually rises through most of the cryogenic range. Hence sample equilibration times drop until temperatures around 10-20 K are reached. Then the mean free path becomes limited by sample dimensions and thermal conductivity drops as T^3 due to its proportionality to specific heat³³. The consequence of this is that fast thermal equilibration can be anticipated in Raman laser-cooling of solids at all but the very lowest ($T < 10$ K) temperatures.

1.5 References

1. Pringsheim P. (1929). Zwei Bemerkungen über den Unterschied von Lumineszenz- und Temperaturstrahlung, *Z. Phys. A* **57**, 739-746.
2. Hansch T.W. and Schawlow A.L. (1975). Cooling of gases by laser radiation, *Opt. Comm.* **13**, 68-69.
3. Landau L. (1946). On the thermodynamics of photoluminescence, *J. Phys. (Moscow)* **10**, 503-506.
4. Ruan X.L., Rand S.C., and Kaviany M. (2007), Entropy and efficiency in laser cooling of solids, *Physical Review B* **75**, 214304(1-9).
5. Ashkin A. and Dziedzic J.M. (1987). Optical trapping and manipulation of viruses and bacteria, *Science* **235**, 1517-1520.
6. Cohadon P.F., Heidmann A., and Pinard M. (1999). Cooling of a mirror by radiation pressure, *Phys. Rev. Lett.* **83**, 3174-3177.
7. See for example Metcalf H. and van der Straten P. (1999). *Laser Cooling and Trapping*, Springer-Verlag, New York.
8. Epstein R.I., Buchwald M.I., Edwards B.C., Gosnell T.R., and Mungan C.E. (1995). Observation of laser-induced fluorescent cooling of a solid, *Nature* **377**, 500-503.
9. See for example Powell R.C. (1998). *Physics of Solid State Laser Materials*, Springer-Verlag, New York, pp. 154.
10. Loudon R., *The Quantum Theory of Light* (2000). 3rd edition, *Oxford University Press*, Oxford, pp. 349.
11. Donovan B. and Angress J.F. (1971). *Lattice Vibrations*, Chapman and Hall, London.
12. Clark J.L., Miller P.F., and Rumbles G. (1998). Red Edge Photophysics of Ethanolic Rhodamine 101 and the Observation of Laser Cooling in the Condensed Phase, *J. Phys. Chem. A* **102**, 4428-4437.
13. Zhang J., Li D., Chen R., and Xiong Q. (2013). Laser cooling of a semiconductor by 40 Kelvin *Nature* **493**, 504-508.
14. Bahl G., Tomes M., Marquardt F. and Carmon T. (2012). Observation of Spontaneous Brillouin Cooling, *Nature Physics* **8**, 203-207.
15. Kittel C. (1971). *Introduction to Solid State Physics*, Fourth Edition, *J. Wiley & Sons*, New York.
16. Sheik-Bahae M. and Epstein R.I. (2007). Optical refrigeration, *Nature Photonics* **1**, 693-699.
17. Pines D. (1964). *Elementary Excitations in Solids*, *W.A. Benjamin, Inc.*, New York, p.232.
18. Shen Y.R. (1984). *The Principles of Nonlinear Optics*, *J. Wiley & Sons*, New York, p. 192.
19. Tomes M., Marquardt F., Bahl G., and Carmon T. (2011). Quantum mechanical theory of optomechanical Brillouin cooling, *Physical Review A* **84**, 063806(1-5).

20. Shen Y.R. and Bloembergen N. (1965). Theory of stimulated Brillouin and Raman scattering, *Physical Review* **137** No. 6A, 1787-1805.
21. Yariv A. (1965). Quantum theory for parametric interactions of light and hypersound, *I.E.E.E. J. Qu. Elect.* **1** No. 1, 28-36.
22. Louisell W.H. (1960). *Coupled Modes and Parametric Electronics*, Wiley, New York.
23. Toschek P.E. (1985). Lumino-refrigeration, *Ann. Phys. (Fr.)* **10**, 761-775.
24. Lindberg M. and Javanainen J. (1986). Temperature of a laser-cooled trapped three-level ion *J.O.S.A. B* **3**, No. 7, 1008-1017.
25. Kasevich M. and Chu S. (1992). Laser cooling below a photon recoil with three-level atoms, *Phys. Rev. Lett.* **69**, 1741-1744.
26. Rand S.C. (2013). Raman laser cooling of solids, *J. Lumin.* **133**, 10-14.
27. Reichel J., Morice O., Tino G.M., and Salomon C. (1994). Subrecoil Raman cooling of Cesium atoms, *Europhys. Lett.* **28**, 477.
28. Reichel J., Bardou F., Ben Dahan M., Peik E., Rand S.C., Salomon C., and Cohen-Tannoudji C. (1995). Raman cooling of Cesium below 3 nK: New approach inspired by Levy Flight Statistics, *Phys. Rev. Lett.* **75**, 4575-4578.
29. See for example Rand S.C. (2015). *Lectures on Light*, 2nd Edition, *Oxford University Press*, Oxford, Appendix G.
30. Kuhn A., Perrin H., Hansel W. and Salomon C. (1997). Three dimensional Raman cooling using velocity selective rapid adiabatic passage, in *OSA TOPS on Ultracold Atoms and BEC*, Vol. **7**, 58-66.
31. Feofilov S.P., Kulinkin A.B., Gacoin T., Mialon G., Dantelle G., Meltzer R.S. and Dujardin C. (2012). Mechanisms for Ce³⁺ excitation at energies below the zero-phonon line in YAG crystals and nanocrystals, *J. Lumin.* **132**, 3082-3088.
32. See Abragam A. and Bleaney B. (1970). *Electron Paramagnetic Resonance of Transition Ions*, *Dover Publications*, New York, pp. 560-562.
33. See for example Kittel C. (1971) *Introduction to Solid State Physics*, 4th edition, *Wiley*, New York, p. 228.